Nanoscale zero-valent iron (nZVI) immobilization onto graphene oxide (GO)-incorporated electrospun polyvinylidene fluoride (PVDF) nanofiber membrane for groundwater remediation via gravity-driven membrane filtration

Jiawei Ren[a,1], Yun Chul Woo[b,1], Minwei Yao[a], Sungil Lim[a], Leonard D. Tijing[a,*], Ho Kyong Shon[a,*]

[a]Centre for Technology in Water and Wastewater, School of Civil and Environmental Engineering, University of Technology Sydney, P. O. Box 123, 15 Broadway, NSW 2007, Australia

[b]Department of Land, Water and Environment Research, Korea Institute of Civil Engineering and Building Technology (KICT), 283, Goyang-Daero, Ilsanseo-Gu, Goyang-Si, Gyeonggi-Do, 10223, Republic of Korea

*Corresponding author: H. K. Shon (Hokyong.Shon-1@uts.edu.au)

[1]J. Ren and Y. C. Woo contributed equally to this work

Abstract

Nanoscale zero-valent iron (nZVI), with its high reactivity towards a broad range of contaminants, has been a promising material for groundwater remediation. Membrane-supported nZVI can both avoid nZVI agglomeration for better reactivity and recycle nZVI to lower the risk of secondary pollution. In this study, we successfully fabricated a PVDF-GO membrane via electrospinning technology and employed the functionalized nanofiber membrane to immobilize nZVI particles. The addition of GO into PVDF nanofibers can both increase the hydrophilicity to improve membrane flux and offer –COOH as a binder to immobilize nZVI particles. PVDF-GO-nZVI membranes with different GO loadings (0%, 0.5%, 1%, 3% of PVDF) were tested with two typical nZVI-targeted contaminants (Cd(II) and trichloroethylene (TCE)) via gravity-driven membrane filtration. The results show that membrane with 1% GO had the best nZVI distribution against the aggregation and a better performance in both Cd removal (100%) and TCE removal (82%). The nZVI membrane had an high flux in gravity-driven filtration at 255LMH for Cd(II) and 265LMH for TCE respectively. Generally, the developed PVDF-GO-nZVI electrospun nanofiber membrane had an excellent performance in the gravity-driven membrane filtration system for groundwater remediation.

Keywords: nano-scale zero valent iron, electrospun nanofiber membrane, graphene oxide, groundwater remediation, gravity-driven membrane filtration

1. Introduction

With the rapid urban and economic development and the growing population, contaminants in groundwater has become complex and intractable. Various pollutants like heavy metals, chlorinated organics and dyes seriously influence the quality and safety of groundwater (Vidmar et al., 2018). Nanoscale zero-valent iron particles (nZVI), with their high reactivity towards a broad range of contaminants, are widely used in groundwater remediation (Tosco et al., 2014). However, nZVI particles themselves are prone to agglomeration, sedimentation and oxidization (Dong et al., 2017; Lefevre et al., 2016). Traditional methods to address these issues are to add surfactants (Kim et al., 2010), suspending agents and stabilizers (Hwang et al., 2014) to maintain the uniformity and activity of nZVI particles distributed in the groundwater. Though nZVIs particles are effective in removing the target pollutants, the adsorbed auxiliary additives and contaminants and the nZVI particles themselves may pose a risk of secondary pollution as long as they remained in groundwater without retrieving them (Dong et al., 2012).

To solve these issues, immobilizing the nZVI particles on a high-surface area membrane substrate would be recycled and potentially reduce the risk of secondary pollution, thus this approach of nZVI particle-loaded membrane is put forward here (Wan et al., 2017). An ideal substrate for nZVI would be a membrane with high specific surface area, recyclable and easily-functionalized properties, which not only can stably immobilize nZVI to avoid agglomeration and sedimentation, but also can recycle nZVI particles or adsorbed contaminants after use (Ren et al., 2017a). Electrospinning is one of the alternative membrane fabrication technologies but has only found its application for nZVI immobilization in recent years due to its low cost, large specific area, size-controllable and easily-functional properties (Ren et al., 2017b). PVA-PAA membrane have been used to immobilize nZVI particles and the PVA-PAA-nZVI membrane

had an excellent removal on trichloroethylene (TCE) (Ma et al., 2012). Liu et al. (Liu et al., 2014) also successfully immobilized nZVI particles onto a polyacrylonitrile (PAN)-based oxidized membrane to reduce water contaminants, which had shown an excellent removal performance. However, these kinds of membranes are lacking mechanical strength (Bichara et al., 2014) or chemical stability (Manavi‐Tehrani et al., 2010) and hard to be employed in a long-term filtration process. Although, in our previous studies (Ren et al., 2017b; Ren et al., 2019), we have successfully improved the immobilization of nZVI and mechanical strength of the PVA-PAA-nZVI membrane, it still had some difficulties in nZVI regeneration due to lack of chemical/ acid-base resistance.

Polyvinylidene fluoride (PVDF) with its strong mechanical strength and excellent chemical stability has already been one of the most commonly-used materials in membrane fabrication (Kang and Cao, 2014). However, PVDF is highly hydrophobic and does not have active functional groups to bind with nZVI particles (Boo et al., 2016). To solve the problem, graphene oxide (GO) with good hydrophilicity and a large number of carboxylic groups (–COOH) could be a good additive to improve membrane hydrophilicity and introduce –COOH onto PVDF membrane for nZVI immobilization (Wang et al., 2014a). Jang et al. (Jang et al., 2015) fabricated PVDF-GO membrane by electrospinning and improved membrane flux due to the introduction of GO in microfiltration process. However, the research on both using PVDF-GO membrane for nZVI immobilization and its application via gravity-driven membrane filtration process has not been reported yet.

Thus, this study aims to fabricate a PVDF-GO nanofiber membrane by electrospinning and the fabricated membrane was used to immobilize nZVI particles by in-situ synthesis method. The effect of GO on membrane fabrication and hydrophilicity were characterized by scanning electron microscopy (SEM), attenuated total reflectance - fourier transform infrared spectroscope (ATR-FTIR), X-ray diffraction (XRD), contact angle and mechanical strength.

The immobilization performance of nZVI was examined by SEM, energy dispersive X-ray spectrometry (EDX), Thermo-gravimetric analysis (TGA), XRD and pore size. Two typical nZVI-targeted contaminants (cadmium (Cd) and TCE, as representatives of heavy metal and chloride organics) were separately filtered by the fabricated PVDF-GO-nZVI membranes via gravity-driven filtration process. The effect of nZVI particles and contaminants on membrane flux and removal performance were tested as well.

2. Materials and methods

2.1 Materials

PVDF (Kynar® 761, Mw = 441,000 g/mol) was purchased from Arkema InC., Australia. Graphene oxide (GO), ferrous sulfate heptahydrate ($FeSO_4 \cdot 7H_2O$), sodium borohydride ($NaBH_4$), cadmium nitrate ($Cd(NO_3)_2$), trichloroethylene (TCE), ethanol and n-hexane were all purchased from Sigma-Aldrich. De-ionized (DI) water from a Millipore Milli-Q water system was used; all the oxygen-free water was prepared by purging nitrogen gas for 10 min to remove the dissolved oxygen and avoid the oxidation of nZVI particles. All chemicals were used as received.

2.2 Solution preparation and electrospinning of PVDF-GO nanofiber membranes

GO particles with different ratios (**Table 1**) were added into a mixed solvent composed of DMF and acetone (3:1 by wt%) at room temperature with sonication for 3 h to make it well-distributed. Then PVDF powders were dissolved into the GO-mixed solvent by stirring for 48 h at room temperature.

The electrospinning set-up is similar to our previous study (Ren et al., 2017b). Nanofibers were directly fabricated onto a rotating drum collector covered with baking paper in a sealed chamber. The feed flow rate was controlled at 1 ml/h by a syringe pump. All the fabricated

mats were electrospun at an employed voltage of 18 kV and the tip-to-collector distance (TCD) was 15 cm.

The polymer solution was supplied by a 12 ml syringe attached with a needle (21G, inner diameter = 0.51 mm) connected via a metallic adaptor. The membranes thickness were controlled at 100 ± 5 μm. The as-spun membranes were dried in oven at 60 °C for 48h to remove the residual solvent.

Table 1. Composition of PVDF-GO solution for electrospinning

Membrane	PVDF (wt%)	GO/PVDF (wt%)	DMF (wt%)	Acetone (wt%)
PVDF	15	0	68	17
PVDF-GO0.5		0.5		
PVDF-GO1		1		
PVDF-GO3		3		

2.3 Synthesis of nZVI on the PVDF-GO membrane

Fig. 1 shows the schematic of the synthesis of nZVI-decorated PVDF-GO membranes. All the PVDF-GO membranes were first filtered with 0.2 mol/L $FeSO_4$ solution for 3 h to allow the complexation of ferrous ions (see **Fig. 1**). After that, all the PVDF-GO-Fe(II) membranes were filtered with 0.5 mol./L $NaBH_4$ solution in an anaerobic chamber (filled by N_2 gas) to form and immobilize nZVI particles. The reaction is shown below (Wang et al., 2008),

$$Fe^{2+} + 2BH_4^- + 6H_2O \rightarrow Fe^0\downarrow + 2B(OH)_3 + 7H_2\uparrow \quad \textbf{(1)}$$

The successful formation of nZVI on the PVDF-GO membrane is indicated by the change of color of the mat into black, and once the black color was stable (~10 mins generation time), the PVDF-GO-nZVI mats were rinsed by ethanol then stored in a sealed glass bottle, which was filled with nitrogen gas.

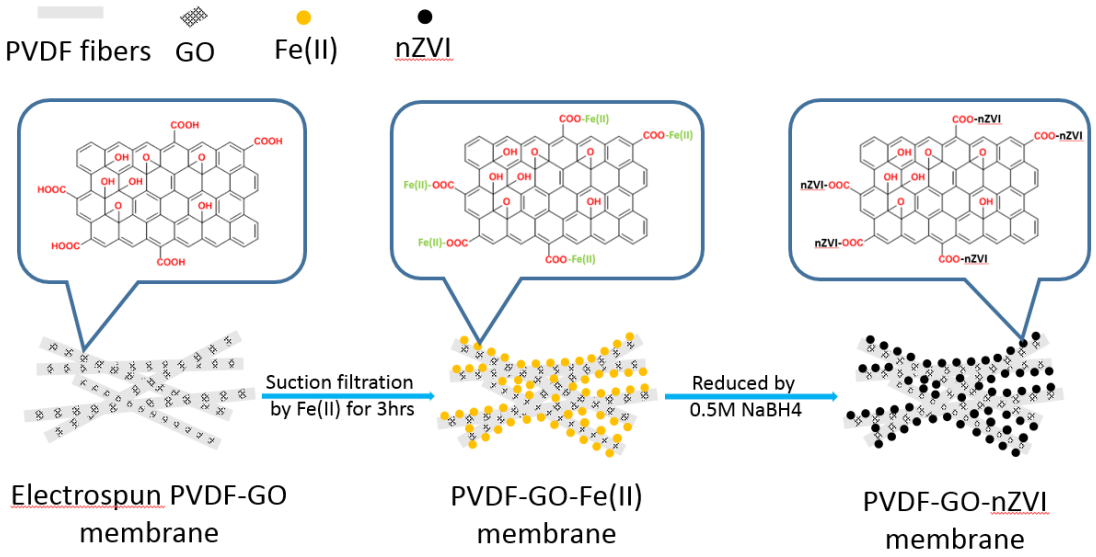

Figure 1. Schematic diagram of the nZVI particles growth and re-immobilization

2.4 Gravity-driven membrane filtration

To test the performance of PVDF-GO-nZVI membranes on a relatively real condition of groundwater remediation, all the membranes were used to filtrate Cd(II) and TCE solutions seperately by a gravity-driven membrane filtration application.

Schematic diagram of the filtration set-up is shown in **Fig. 2**. The thickness of each mat was controlled at 100 ± 10 μm and the area for filtration was 14 cm^2. The initial Cd(II) concentration was 20 mg/L and 100 ml solution was filtered in each filtration cycle (5 cycles for 500 mL in total). 10 mL permeated sample was withdrawn after each filtration cycle for the analysis of Cd(II) concentration via microwave plasma-atomic emission spectrometry (4100 MP-AES, Agilent Technologies, US). Removal efficiency to Cd(II) was determined using the following equation:

$$\text{Removal efficiency (\%)} = \frac{C_{int} - C_{end}}{C_{int}} \times 100\% \quad \textbf{(2)}$$

where, C_{int} and C_{end} refer to the initial and final Cd(II) concentrations, respectively.

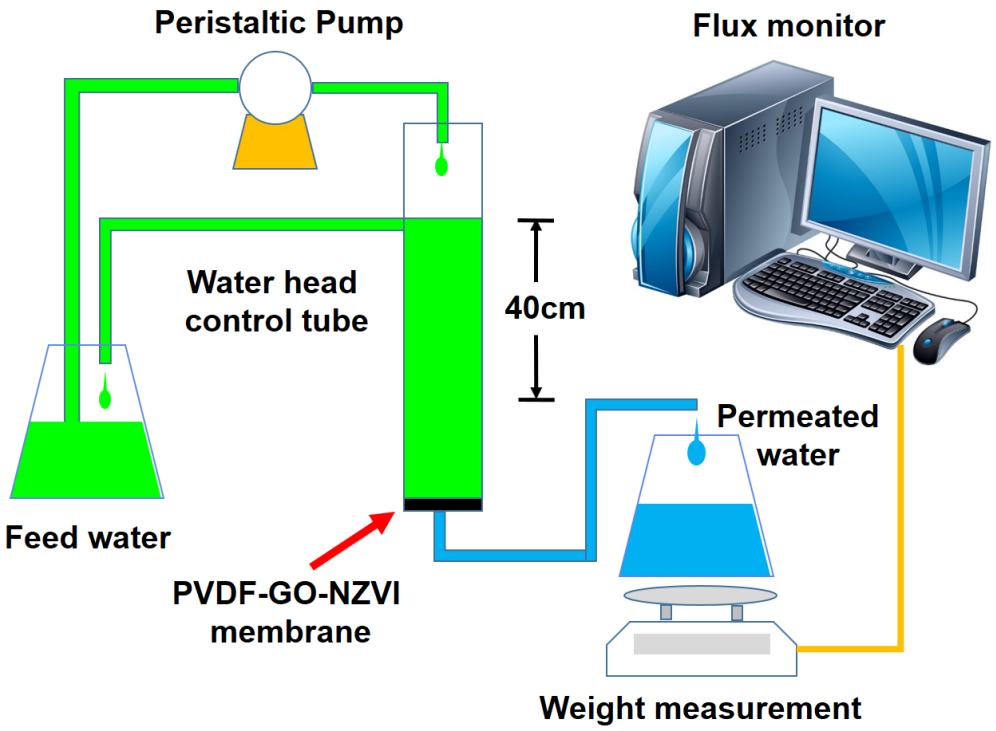

153

154 **Figure 2.** Schematic diagram of nZVI membrane gravity-driven filtration system

155 In addition, TCE as a typical chloride organic was also selected to test the dechlorination
156 capacity of PVDF-GO-nZVI membrane. Similarly, the concentration of TCE was also 20 mg/L
157 but the permeated sample was withdrawn and transferred to a new vial for the subsequent
158 liquid-liquid extraction. The chemical n-hexane was used to extract TCE from water. The
159 concentration of the extracted TCE solution was measured by GC-MS-TQ8040 (Shimadzu,
160 Japan). The removal efficiency was calculated using the following equation:

161 $$\text{TCE removal efficiency (\%)} = \frac{C_{\text{int}} - C_{\text{end}}}{C_{\text{int}}} \times 100\% \quad \textbf{(3)}$$

162 where, C_{int} and C_{end} are the initial and the final TCE concentrations, respectively.

163 **2.5 Membrane Characterizations**

164 Membrane surface morphology and element component analysis were measured by scanning
165 electron microscopy and energy dispersive X-ray spectrometry (SEM and EDX, Zeiss Supra
166 55VP, Carl Zeiss AG). All the fiber/particle sizes and distributions were measured by Image J.

Thermo-gravimetric analysis (TGA) was measured by Discovery TGA thermo-gravimetric analyzer (SDT-Q600, US) from 80°C to 800°C at a heating rate of 10°C/min in N_2 atmosphere [27]. The functional groups of membranes/particles were analyzed by attenuated total reflectance Fourier transform infrared spectroscopy (ATR-FTIR) via Paragon 1000 Spectrometer (PerkinElmer, USA), wavelength from 600 to 4000 cm-1 with a minimum of 40 scans. X-Ray diffraction (XRD) (Siemens D5000) was carried out over Bragg angles ranging from 1° to 80° (Cu Kα, λ=1.54059Å) (Woo et al., 2016). The mechanical properties of different membrane samples were measured using a Universal Testing Machine (UTM, Lloyd), equipped with a 1 kN load cell. The test was conducted using a constant elongation velocity of 5 mm/min under room temperature (Woo et al., 2017). Galwick (surface tension of 15.9 mN/m) was used to wet the membranes in pore size. Each sample was first applied with N_2 gas to measure the gas permeability. A sessile drop method utilizing Theta Lite 100 (Attension, Sweden) with built-in software was used to analyses the contact angles of all the membranes (Yao et al., 2019). A water droplet around 5 µl was released from a needle tip onto the membrane surface. A motion camera was mounted to take photos at a rate of 12 frames per second. Each sample was measured for three times and the average value was taken.

3. Results and discussion

3.1 Effect of GO on PVDF membranes

Fig. 3 shows the SEM images and fiber size distributions of as-spun PVDF-GO nanofiber membranes with different GO ratios. All the membranes showed bead-less and defect-free cylindrical nanofiber structure. The average fiber sizes of the as-spun membranes (PVDF, PVDF-GO0.5, PVDF-GO1 and PVDF-GO3) were 167 ± 79, 259 ± 129, 311 ± 131 and 355 ± 237 nm, respectively. It is clear that the fiber size increased with the increase in the GO added

into the PVDF solution. However, the addition of GO broke the continuity of polymer jetting during the electrospinning, which resulted to a wider fiber size distribution. Similar results were also reported in previous studies (Jang et al., 2015).

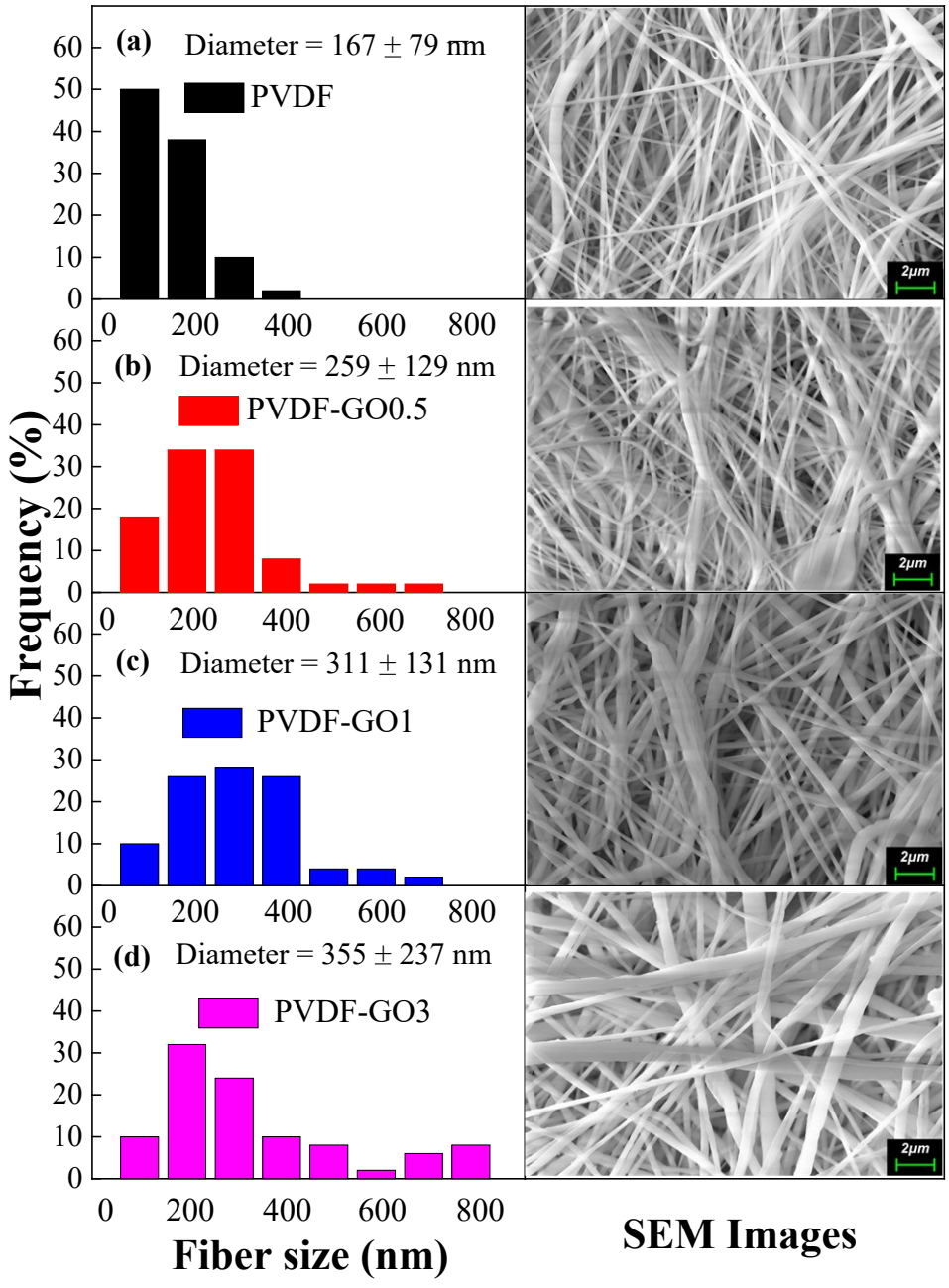

Figure 3. Surface SEM images and corresponding fiber size distributions of (a) PVDF; (b) PVDF-GO0.5; (c) PVDF-GO1 and (d) PVDF-GO3 electrospun nanofiber membranes

Fig. 4 shows the ATR-FTIR spectra of the PVDF-GO membranes. For the pristine PVDF, the characteristic absorption band is mainly in the wavenumber region of 840 – 1402 cm^{-1}. Specifically, the peak intensities at 1181, 1275 cm^{-1} represents symmetrical stretching of –CF and $-CF_2$ stretching, while peaks at 840, 883, 1070 and 1402 cm^{-1} represents the $-CH_2$ rocking, $-CH_2$ wagging of vinylidene, bending of −CH bond and the stretching vibration of C-H bonds (Ghaffar et al., 2018; Zeng et al., 2016) respectively. In terms of GO membranes, The peaks at 1622, 1720 and 3500 cm^{-1} indicated the existence of C=C, -COOH and -OH, which proved the deposition of GO onto the PVDF membrane (Ghaffar et al., 2018). With the increase of GO ratio, the peak of –COOH and C-OH increased correspondingly but the characteristic peaks of PVDF reduced due to the ratio of PVDF in the composite reduced as well. The XRD results of all the electrospun membranes are presented in **Fig. 5**. There are clear peaks at $2\theta = 10.5^{o}$ on all the PVDF-GO membranes indicating the existence of GO. The peak intensity increased with the increase of GO/PVDF ratio and PVDF-GO3 had the highest GO peak intensity, which was consistent with FTIR results (**Fig. 4**).

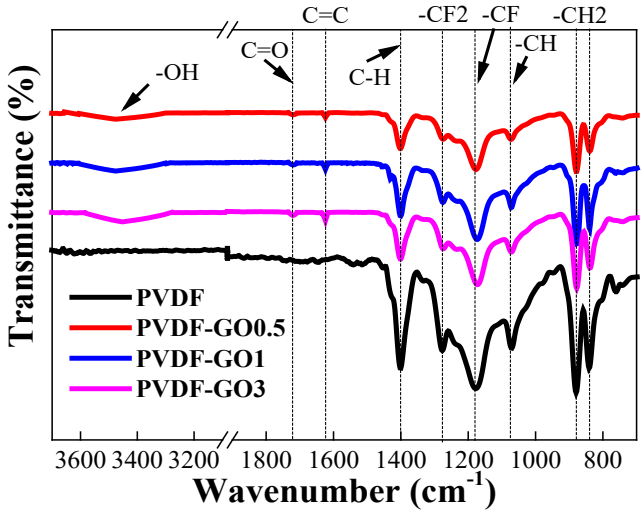

Figure 4. ATR-FTIR spectra of all the PVDF-GO elelctrospun nanofiber membranes

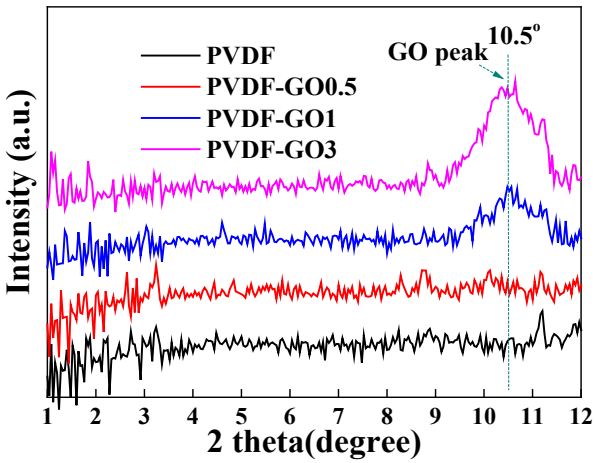

212

213 **Figure 5.** XRD patterns of all the PVDF-GO elelctrospun nanofiber membranes

214 A contact angle measurement was conducted on the PVDF-GO membranes and the results
215 are shown in **Fig. 6**. The pristine PVDF membrane showed the highest contact angle of 140±
216 1.9°, indicating being highly hydrophobic. Expectedly, the addition of GO nanoparticles
217 significantly reduced the contact angle of PVDF membrane, because the –COOH and -OH on
218 GO are hydrophilic. With the increase of GO ratio, the average contact angle reduced from
219 140° to 110° and the PVDF-GO3 had the lowest contact angle at 110±4.2° .

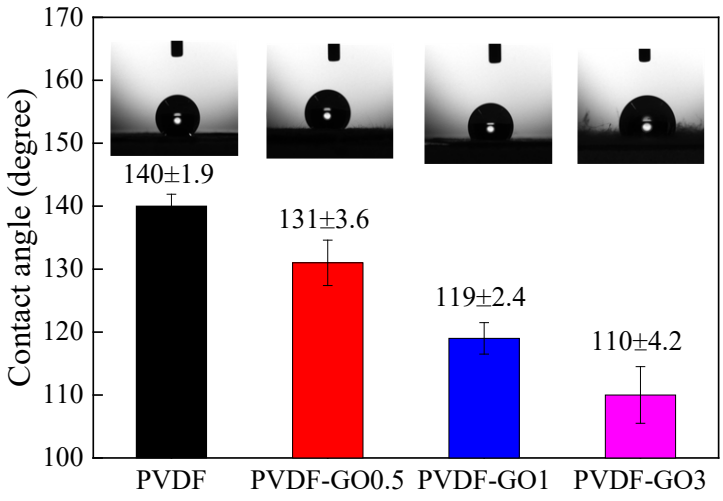

220

221 **Figure 6.** Contact angles of all the PVDF-GO electrospun nanofiber membranes

222

223 **Table 2.** Mechanical properties of the neat PVDF and PVDF-GO electrospun nanofiber
224 membranes

	Tensile strength (MPa)	Strain (%)	Young's modulus (MPa)
PVDF	6.4	49.3	13
PVDF-GO0.5	5.2	27	19.3
PVDF-GO1	4.8	12.6	38.1
PVDF-GO3	4.4	9.5	46.3

225

226 The mechanical properties of the neat PVDF membrane and the PVDF-GO membranes are
227 presented in **Table 2**. It is obvious that the addition of GO led to a decrease of the tensile
228 strength as well as the percentage of the strain. With the increase of GO ratio in the
229 membrane, the tensile strength decreased from 6.4 MPa to 4.4 MPa and the strain reduced
230 from 49.3% to 9.5%. However, the Young's modulus increased from 13 MPa to 46.3 MPa,
231 which means the more GO added, the more plastic the nanocomposites will be. Although the
232 PVDF-GO membranes became more plastic, they had a better resistance to deformation of
233 fiber structure (Ren et al., 2019).

234 **3.2 Immobilization of nZVI onto PVDF-GO membrane**

235 The surface SEM images of all the nZVI-immobilized PVDF-GO membranes are shown
236 in **Fig.7**. It is clear that nZVI nanoparticles have been successfully generated on each PVDF-
237 GO membrane. However, the neat PVDF membrane without GO did not show a good
238 immobilization of nZVI due to the lack of functional groups and only a few nZVI particles
239 were stuck among fibers via physical interaction other than chemical bonding. With the
240 increase of GO content in PVDF nanofiber, nZVI immobilized on PVDF-GO membranes
241 increased as well. It is noticed that although PVDF-GO3 seemed to have the most nZVI
242 particles immobilized onto nanofibers, the particles were more aggregated and not well-
243 distributed (**Fig. 7c**). Specifically, nZVI particles were more immobilized on the thin fibers
244 than thicker fibers. This is due to the fact that the functional moieties (-COOH) are mainly on

245 the edge of GO and the edges of GO are more likely to pierce the surface of thinner fibers
246 rather than encapsulated inside the thicker fiber (Hu et al., 2016). **Fig. 7e** shows the Fe/C weight
247 ratio of each nZVI membrane by EDS analysis in the SEM images and the results are highly
248 consistent with the SEM images. The Fe/C ratio of neat PVDF was extremely low at 0.02,
249 approximately 1/50 lower than those on PVDF-GO membranes, which indicates that the neat
250 PVDF membrane failed to immobilize nZVI particles. In contrast to PVDF-GO membranes,
251 with the ratio of GO added into PVDF membrane, the Fe/C ratio increased significantly.
252 PVDF-GO3-nZVI (**Fig. 7d**) had the highest Fe/C ratio at 2.03 on its membrane surface, around
253 1.5 times higher than that on PVDF-GO1-nZVI (**Fig. 7c**).

254

255

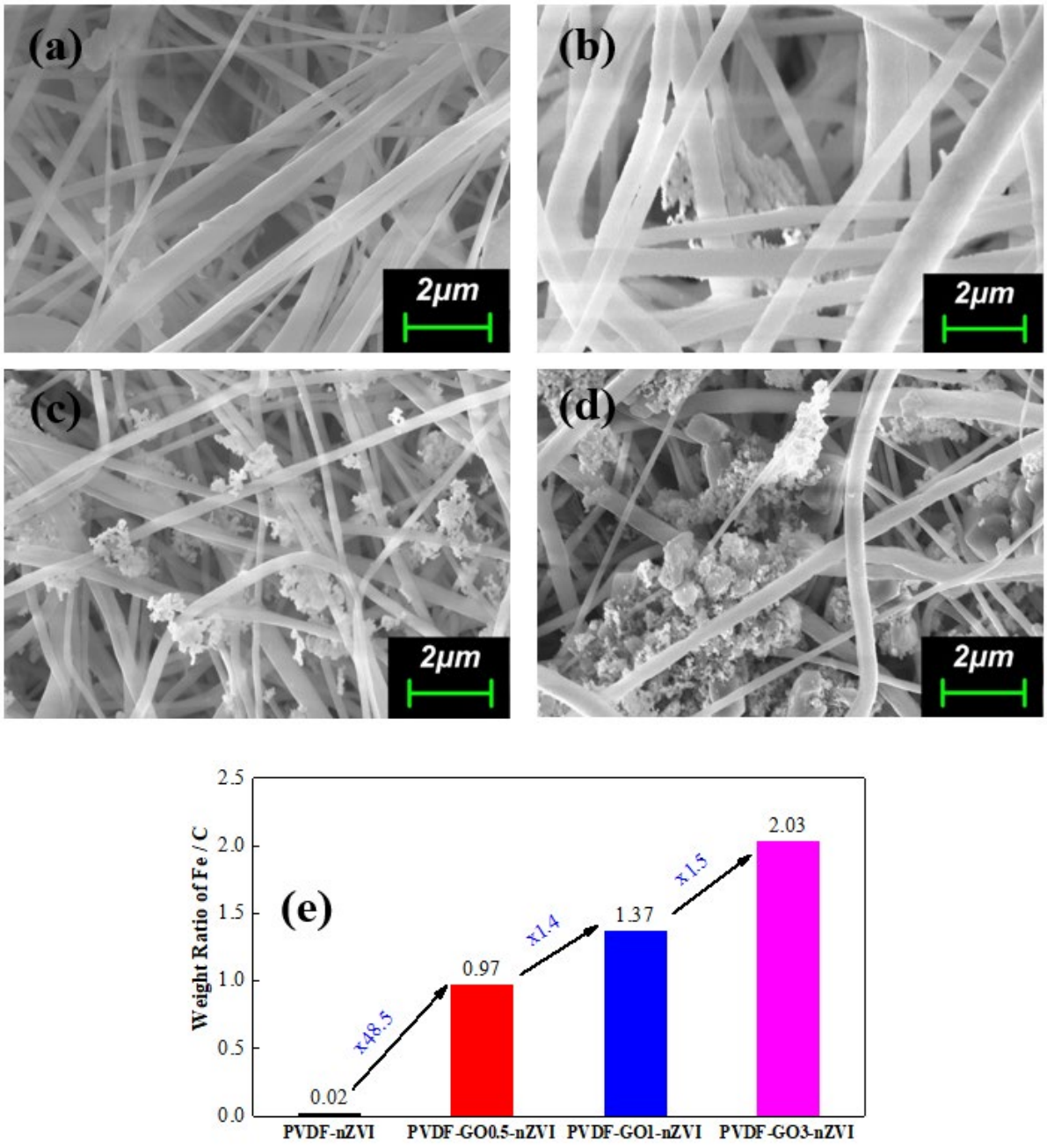

256

257 **Figure 7.** Surface SEM images of: (a) PVDF-nZVI; (b) PVDF-GO0.5-nZVI; (c) PVDF-GO1-
258 nZVI; (d) PVDF-GO3-nZVI electrospun nanofiber membranes; and (e) the weight ratio of
259 Fe/C on the surface of the four nZVI-immobilized electrospun nanofiber membranes based
260 from EDS analysis.

261 The pore size of PVDF-GO membranes before and after nZVI immobilization are
262 presented in **Table 3**. Before the immobilization of nZVI, the mean pore size increased with
263 the GO content (from 0.8 μm to 1.21 μm) due to the increase of fiber size (Wang et al., 2014b).

After nZVI immobilization, all the membrane pore sizes decreased and the pore size of the membrane with a higher GO ratio reduced more significantly. This is mainly because the nZVI particles were deposited on the surface of fibers and then occupied the voids among the fibers. Membrane with high GO ratio immobilized more nZVI particles and hence the pore size reduced more.

Table 3. Mean pore sizes of PVDF-GO membranes before/after nZVI immobilization

	Mean pore size (μm)		Mean pore size (μm)
PVDF	0.8	PVDF-nZVI	0.79
PVDF-GO0.5	0.99	PVDF-GO0.5-nZVI	0.95
PVDF-GO1	1.13	PVDF-GO1-nZVI	1.06
PVDF-GO3	1.21	PVDF-GO3-nZVI	1.11

The cross-sectional SEM images of all the nZVI-immobilized PVDF-GO membranes and their Fe/C ratios are shown in **Fig. 8.** Only very few nZVI particles immobilized onto the neat PVDF-nZVI (**Fig. 8a**) and PVDF-GO0.5-nZVI (**Fig. 8b**) membranes. Correspondingly, their Fe/C ratios were lower than those on their surfaces. This is mainly caused by the stronger hydrophobicity (higher contact angles, **Fig. 6**) and the smaller mean pore sizes of PVDF and PVDF-GO1 (0.8 and 0.99 μm respectively, **Table 3**). After forming nZVI particles on the membrane surface, the mean pore size became smaller and reducing agent cannot evenly penetrate the hydrophobic PVDF and PVDF-GO0.5 membranes. As a result, only few nZVI particles were immobilized inside the membrane. However, the immobilization of nZVI particles inside PVDF-GO1-nZVI (**Fig. 8c**) was as much as the nZVI on its surface (**Fig. 7c**), which means the nZVI particles were uniformly distributed on the whole PVDF-GO1-nZVI. Meanwhile, its Fe/C weight ratio on cross-section (**Fig. 8e**) was also same as the result on surface measurement (**Fig. 7e**), which proved the high uniformity of nZVI immobilized onto the PVDF-GO1-nZVI as well. In terms of PVDF-GO3-nZVI, due to the aggregation of nZVI

285 on the surface (**Fig. 7d**), its pore size decreased significantly by nZVI blocking and hence
286 hindering the generation of nZVI inside the membrane, leading to a lower Fe/C ratio inside.

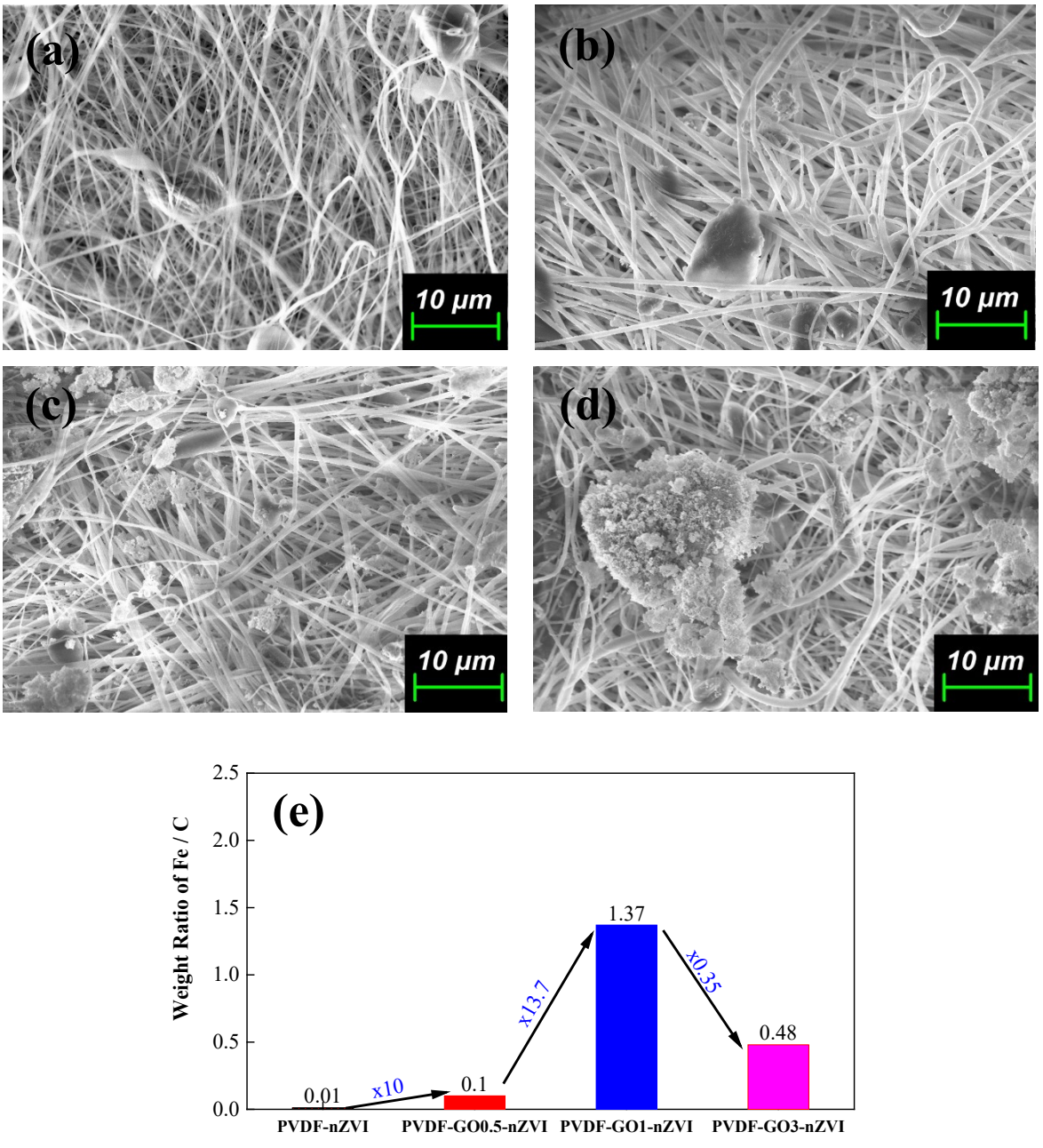

287

288 **Figure 8.** Cross-sectional SEM images of (a) PVDF-nZVI; (b) PVDF-GO0.5-nZVI; (c) PVDF-
289 GO1-nZVI; (d) PVDF-GO3-nZVI electrospun nanofiber membranes and (e) the weight ratio
290 of Fe/C on the cross-sectional of the four nZVI immobilized electrospun nanofiber membranes

291 XRD results of nZVI-incorporated PVDF-GO electrospun nanofiber membranes are
292 presented in **Fig. 9**. The peak at 45° represents the crystal structure of α-Fe (110), indicating

the existence of nZVI onto PVDF-GO membranes (Gu et al., 2018), although the intensity of the peak was not very high due to a less mass ratio of nZVI on the nanocomposites and the strong peak of amorphous structure of PVDF-GO electrospun nanofiber membranes.

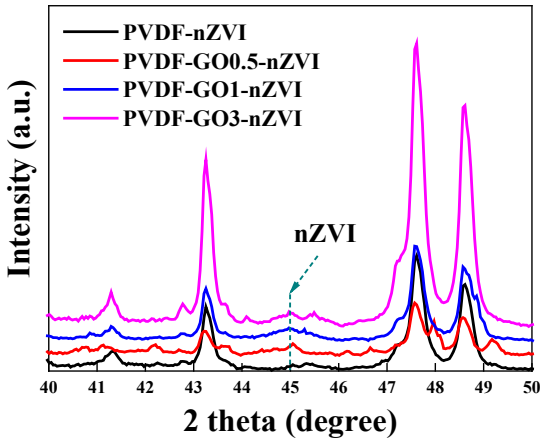

Figure 9. XRD pattern of all the PVDF-GO-nZVI electrospun nanofiber membranes

TGA was used to characterize the loading capacity of nZVI particles immobilized onto the dual-crosslinked nanofiber membranes (**Fig. 10**). The weight loss on each membrane on the temperature range from 150 to 400℃ indicates the decomposition of GO (Issa et al., 2016; Şinoforoğlu et al., 2013). Afterwards, the major weight loss at the region from 400 to 500℃ is attributed to the decomposition of the PVDF polymers(Thakur et al., 2011). Obviously, the neat PVDF without GO decreased the most weight percentage.

At 800℃, all the polymeric nanofibers had already been decomposed, leaving carbons and nZVI particles as the residual mass (Sharma et al., 2015). Neat PVDF remained only carbon and few nZVI particles at 9.6 wt%. PVDF-GO3 immobilized the most nZVI with about 37.8 wt%, while PVDF-GO1 immobilized the second most nZVI around 33.1 wt%, around 28.2% and 23.5% higher than the neat PVDF. Basically, PVDF with a higher GO ratio immobilized more nZVI particle, which is consistent with SEM results.

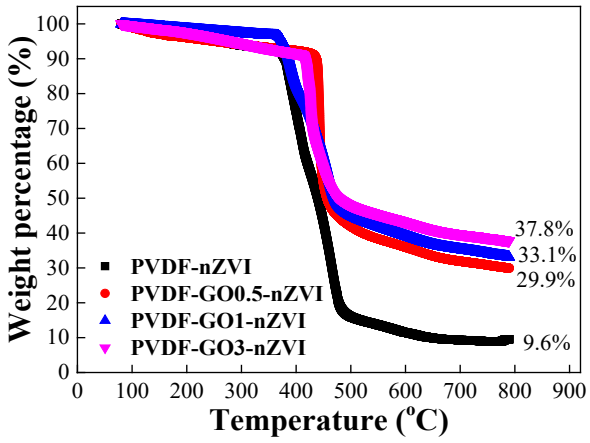

311

312 **Figure 10.** TGA of all the PVDF-GO-nZVI electrospun nanofiber membranes

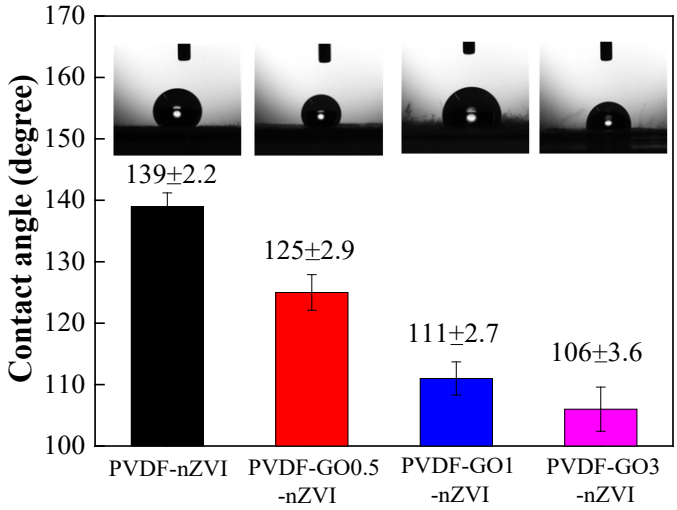

313

314 **Figure 11.** Contact angles of all the PVDF-GO-nZVI electrospun nanofiber membranes

315 Contact angles after nZVI immobilization on the membranes are presented in **Fig. 11**.
316 All the membranes reduced contact angle after nZVI immobilization due to the hydrophilicity
317 of the oxide shell on the nZVI surface. With the least nZVI immobilized, the PVDF-nZVI
318 remained the highest contact angle at 139±2.2°. There is relative larger improvement of
319 hydrophilicity on PVDF-GO membranes. The contact angle of PVDF-GO0.5-nZVI was 125±
320 2.9°, around 6° lower than that before nZVI immobilization. PVDF-GO1-nZVI was improved
321 the most, whose contact angle reduced by 8° from 119±2.4° to 111±2.7°. However, the
322 contact angle of PVDF-GO3-nZVI only decreased around 4° which did not show a better

improvement than PVDF-GO1-nZVI. Although PVDF-GO3 membrane immobilized the most amount of nZVI particles, those nZVI particles are more aggregated, leading to increase surface roughness, which can only improve the hydrophilicity on the part where the nZVI particles gathered.

3.3 Performance of PVDF-GO-nZVI membrane in removing contaminants via gravity-driven membrane filtration

All the nZVI-immobilized electrospun nanofiber membranes were tested via gravity-driven membrane filtration, with water head controlled at 0.4 m. Two typical nZVI-targeted contaminants (Cd(II) and TCE) were employed to test the permeability and removal performance of nZVI-immobilized electrospun nanofiber membranes.

Fig. 12 shows the evolution of flux and Cd(II) removal with the increase of filtration volume. The flux of each membrane decreased with the filtration of Cd(II) solution (**Fig. 12a**). PVDF-nZVI (i.e., without GO) had the lowest flux (from 98 LMH to 70 LMH) among the four membranes due to the smallest membrane pore size and the strongest hydrophobicity. In contrast, with the increase of GO content, the mean pore size and the hydrophilicity of PVDF-GO membranes increased remarkably, thereby contributing to a better permeability. PVDF-GO3-nZVI had the highest initial flux at 269 LMH followed by PVDF-GO1-nZVI at 255 LHM. However, the flux of PVDF-GO3-nZVI declined significantly. After 100 mL filtration, the flux of PVDF-GO3-nZVI was lower than that of PVDF-GO1-nZVI. This is because, with the adsorption of Cd(II) on the surface of nZVI particles, the size-increased nZVI made the membrane pore volume and pore size reduced. Furthermore, nZVI particles on the PVDF-GO3 are more aggregated and hence the pore size reduced more significantly. In **Fig. 12b**, the PVDF-nZVI had a very little removal lower than 8% over the whole filtration test while all the PVDF-GO-nZVI membranes had 100% initial removals of Cd(II). PVDF-GO1-nZVI kept the

excellent removals higher than 90% within 300ml filtration test and after 400 ml, it started to decline and eventually became lower than 10%. However, PVDF-GO0.5-nZVI and PVDF-GO3-nZVI started to decline since 100 ml and 200 ml respectively. After 300 ml filtration, both their removals were lower than 10%. Compared with PVDF-GO1-nZVI, on one hand, PVDF-GO0.5-nZVI did not immobilize enough nZVI to adsorb more Cd(II); On the other hand, although PVDF-GO3-nZVI successfully immobilized more weight of nZVI on the surface, most of them were too aggregate to expose to Cd(II) and hence failed to remain a high removal. The main mechanism of Cd(II) removal by nZVI is chemisorption (bidentate inner-sphere surface complexation) (Boparai et al., 2013). Therefore**,** Cd(II) was adsorbed on the surface of nZVI in the form of ions, specifically $CdFe_2O_4$ reported in previous study (Hidalgo et al., 2015). With the increase of filtration volume, the reaction sites of nZVI was covered by $CdFe_2O_4$ (**Fig. 14a)** and hence the removal reduced. As a result, the particle size should increase and lead to a decline of flux.

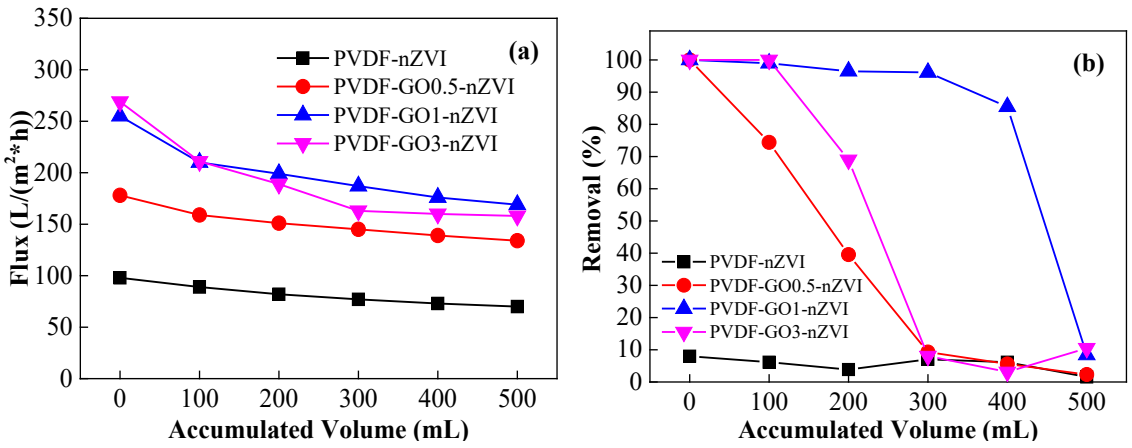

Figure 12. Performances of PVDF-GO-nZVI electrospun nanofiber membranes in gravity-driven membrane filtration test for Cd(II) removal: (a) Flux and (b) Cd(II) removal ratio

In terms of TCE filtration test (**Fig. 13**), the flux of each membrane (**Fig. 13a**) was obviously higher than the flux in Cd(II) filtration test (**Fig. 12a**). Meanwhile, the flux decline of each nZVI membrane in TCE filtration was slower than those in Cd filtration. These could be respectively explained by the followed two reasons: (1) TCE itself is a hydrophobic liquid

(Kiruthika et al., 2014), which has a similar hydrophobicity with the PVDF fibers (Woo et al., 2016). Therefore, it had a higher flux for TCE than Cd(II) solution (2) In contrast to the adsorption of nZVI to Cd(II), the mechanism of TCE removal was the dechlorination process (**Fig. 14b**), which means TCE would not deposit on the surface of nZVI particles. It is reported that TCE was first broken by electron attack originating from the surface of nZVI, and dichloroethylenes (DCE) are formed as intermediates (Tian et al., 2018). Subsequently, DCE was dechlorinated to vinyl chloride (VC) and eventually all dichloroethylene formed was completely dechlorinated to ethylene and ethane (Hara et al., 2005). nZVI was reduced to $Fe(OH)_2$ in the anaerobic groundwater ambience (Tian et al., 2018). Therefore, TCE molecule would not adsorb on nZVI surface and hence remained higher pore sizes, fluxes and removal. Particularly, PVDF-GO3-nZVI with the largest mean pore size had the highest initial flux at 317 LMH and PVDF-nZVI with the smallest mean pore size had the lowest initial flux at 123 LMH. It is noticed that the flux of PVDF-GO1-nZVI is just a bit lower than that of PVDF-GO3-nZVI but much higher than those of PVDF-GO0.5-nZVI and PVDF-nZVI. Nevertheless, the PVDF-GO3-nZVI had a higher pore size, its flux is still limited by the undesirable aggregation of nZVI. On the other hand, the TCE removals of all the membranes (**Fig. 13b**) were obviously lower than their removals for Cd(II) (**Fig.12b**). This may be caused by two reasons: 1) the higher flux of membrane made TCE molecules have less hydraulic retention time to contact and react with nZVI particles. 2) The dechlorination process of TCE was multi-steps (**Fig.14b**), which had a lower total reaction rate than Cd(II) and requires more reaction time. Specifically, PVDF-nZVI had the lowest removal no more than 4% over the whole filtration test and PVDF-GO0.5-nZVI had a very little removal lower than 10% after 100ml. In contrast, PVDF-GO1-nZVI had the highest removal at 82% at the 100 ml. Although PVDF-GO3-nZVI had a slightly higher flux over 500 ml, PVDF-GO1-nZVI with the overwhelming

removal had a better performance in the filtration test. Generally, PVDF-GO1-nZVI had the best performance in gravity-driven filtration test for either Cd(II) removal or TCE removal.

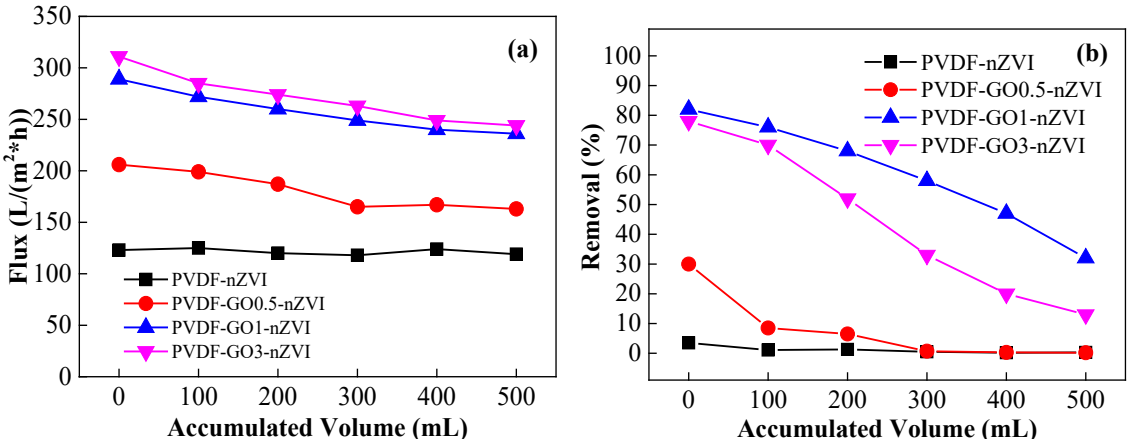

Figure 13. Performances of PVDF-GO-nZVI electrospun nanofiber membranes in gravity-driven membrane filtration test for TCE removal: (a) Flux and (b) TCE removal ratio

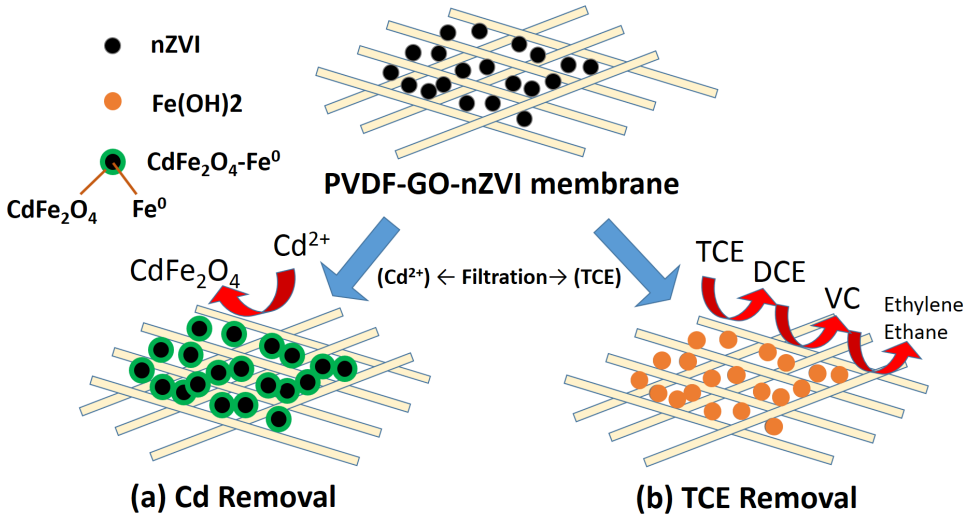

Figure 14. Mechanism of (a) Cd^{2+} and (b) TCE removal by PVDF-GO-nZVI electrospun nanofiber membranes

4. Concluding remarks

In this study, we successfully fabricated PVDF-GO-nZVI membranes via electrospinning technique and developed nZVI electrospun nanofiber membranes were tested with two typical nZVI-targeted contaminants (Cd(II) and TCE) via gravity-driven membrane filtration application. The main conclusions are listed as below:

- GO can introduce functional groups (-COOH) to immobilize nZVI particles as well as improve membrane hydrophilicity to increase filtration flux.
- The more ratio of GO added in PVDF membrane, the more nZVI can be immobilized, but too high GO ratio could make an uneven fiber size distribution in electrospinning process and hence can lead to nZVI aggregation.
- For Cd removal, as the adsorption mechanism made the Cd(II) deposited on the surface of nZVI, PVDF-GO1-nZVI had a better nZVI distribution against the agglomeration, leading to a better removal (100%) and flux (255 LMH).
- For TCE removal, although PVDF-GO3-nZVI had a slightly higher flux (317 LMH), PVDF-GO1-nZVI with the overwhelming removal (82%) had a better performance in the filtration test.

Acknowledgement

This research was funded by the Cooperative Research Centre for Contamination Assessment and Remediation of the Environment (CRC CARE, Project No. 4.1.18-13/14). This research was also funded by Korea Institute of Civil Engineering and Building Technology (KICT) (KICT20190397).

References

Bichara DA, Bodugoz-Sentruk H, Ling D, Malchau E, Bragdon CR, Muratoglu OK. Osteochondral defect repair using a polyvinyl alcohol-polyacrylic acid (PVA-PAAc) hydrogel. Biomedical Materials 2014; 9: 045012.

Boo C, Lee J, Elimelech M. Omniphobic polyvinylidene fluoride (PVDF) membrane for desalination of shale gas produced water by membrane distillation. Environmental science & technology 2016; 50: 12275-12282.

Boparai HK, Joseph M, O'Carroll DM. Cadmium (Cd 2+) removal by nano zerovalent iron: surface analysis, effects of solution chemistry and surface complexation modeling. Environmental Science and Pollution Research 2013; 20: 6210-6221.

Dong H, Guan X, Lo IM. Fate of As (V)-treated nano zero-valent iron: determination of arsenic desorption potential under varying environmental conditions by phosphate extraction. Water research 2012; 46: 4071-4080.

Dong H, Zhao F, He Q, Xie Y, Zeng Y, Zhang L, et al. Physicochemical transformation of carboxymethyl cellulose-coated zero-valent iron nanoparticles (nZVI) in simulated groundwater under anaerobic conditions. Separation and Purification Technology 2017; 175: 376-383.

Ghaffar A, Zhang L, Zhu X, Chen B. Porous PVdF/GO Nanofibrous Membranes for Selective Separation and Recycling of Charged Organic Dyes from Water. Environmental science & technology 2018; 52: 4265-4274.

Gu M, Farooq U, Lu S, Zhang X, Qiu Z, Sui Q. Degradation of trichloroethylene in aqueous solution by rGO supported nZVI catalyst under several oxic environments. Journal of hazardous materials 2018; 349: 35-44.

445 Hara J, Ito H, Suto K, Inoue C, Chida T. Kinetics of trichloroethene dechlorination with iron
446 powder. Water Research 2005; 39: 1165-1173.
447 Hidalgo KTS, Guzmán-Blas R, Ortiz-Quiles EO, Fachini ER, Corchado-García J, Larios E, et
448 al. Highly organized nanofiber formation from zero valent iron nanoparticles after
449 cadmium water remediation. Rsc Advances 2015; 5: 2777-2784.
450 Hu M, Zheng S, Mi B. Organic fouling of graphene oxide membranes and its implications for
451 membrane fouling control in engineered osmosis. Environmental science & technology
452 2016; 50: 685-693.
453 Hwang Y, Lee Y-C, Mines PD, Huh YS, Andersen HR. Nanoscale zero-valent iron (nZVI)
454 synthesis in a Mg-aminoclay solution exhibits increased stability and reactivity for
455 reductive decontamination. Applied Catalysis B: Environmental 2014; 147: 748-755.
456 Issa AA, Mariam Al Ali S, Mrlík M, Luyt AS. Electrospun PVDF graphene oxide composite
457 fibre mats with tunable physical properties. Journal of Polymer Research 2016; 23: 232.
458 Jang W, Yun J, Jeon K, Byun H. PVdF/graphene oxide hybrid membranes via electrospinning
459 for water treatment applications. RSC Advances 2015; 5: 46711-46717.
460 Kang G-d, Cao Y-m. Application and modification of poly (vinylidene fluoride)(PVDF)
461 membranes–a review. Journal of Membrane Science 2014; 463: 145-165.
462 Kim H, Hong H-J, Jung J, Kim S-H, Yang J-W. Degradation of trichloroethylene (TCE) by
463 nanoscale zero-valent iron (nZVI) immobilized in alginate bead. Journal of hazardous
464 materials 2010; 176: 1038-1043.
465 Kiruthika S, Gupta R, Rao K, Chakraborty S, Padmavathy N, Kulkarni GU. Large area solution
466 processed transparent conducting electrode based on highly interconnected Cu wire
467 network. Journal of Materials Chemistry C 2014; 2: 2089-2094.
468 Lefevre E, Bossa N, Wiesner MR, Gunsch CK. A review of the environmental implications of
469 in situ remediation by nanoscale zero valent iron (nZVI): behavior, transport and

impacts on microbial communities. Science of the Total Environment 2016; 565: 889-901.

Liu C, Li X, Ma B, Qin A, He C. Removal of water contaminants by nanoscale zero-valent iron immobilized in PAN-based oxidized membrane. Applied Surface Science 2014; 321: 158-165.

Ma H, Huang Y, Shen M, Guo R, Cao X, Shi X. Enhanced dechlorination of trichloroethylene using electrospun polymer nanofibrous mats immobilized with iron/palladium bimetallic nanoparticles. Journal of hazardous materials 2012; 211: 349-356.

Manavi‐Tehrani I, Rabiee M, Parviz M, Tahriri MR, Fahimi Z. Preparation, Characterization and Controlled Release Investigation of Biocompatible pH‐Sensitive PVA/PAA Hydrogels. Macromolecular symposia. 296. Wiley Online Library, 2010, pp. 457-465.

Ren J, Tijing LD, Shon HK. "Robbing behavior" and re-immobilization of nanoscale zero-valent iron (nZVI) onto electrospun polymeric nanofiber mats for trichloroethylene (TCE) remediation. Separation and Purification Technology 2017a; 189: 375-381.

Ren J, Woo YC, Yao M, Tijing LD, Shon HK. Enhancement of nanoscale zero-valent iron immobilization onto electrospun polymeric nanofiber mats for groundwater remediation. Process Safety and Environmental Protection 2017b; 112: 200-208.

Ren J, Yao M, Woo YC, Tijing LD, Kim J-H, Shon HK. Recyclable nanoscale zerovalent iron (nZVI)-immobilized electrospun nanofiber composites with improved mechanical strength for groundwater remediation. Composites Part B: Engineering 2019.

Sharma AK, Kumar R, Mittal S, Hussain S, Arora M, Sharma RC, et al. In situ reductive regeneration of zerovalent iron nanoparticles immobilized on cellulose for atom efficient Cr (VI) adsorption. RSC Advances 2015; 5: 89441-89446.

493 Şinoforoğlu M, Gür B, Arık M, Onganer Y, Meral K. Graphene oxide sheets as a template for
494 dye assembly: graphene oxide sheets induce H-aggregates of pyronin (Y) dye. Rsc
495 Advances 2013; 3: 11832-11838.
496 Thakur VK, Tan EJ, Lin M-F, Lee PS. Poly (vinylidene fluoride)-graft-poly (2-hydroxyethyl
497 methacrylate): a novel material for high energy density capacitors. Journal of Materials
498 Chemistry 2011; 21: 3751-3759.
499 Tian H, Liang Y, Zhu T, Zeng X, Sun Y. Surfactant-enhanced PEG-4000-NZVI for
500 remediating trichloroethylene-contaminated soil. Chemosphere 2018; 195: 585-593.
501 Tosco T, Papini MP, Viggi CC, Sethi R. Nanoscale zerovalent iron particles for groundwater
502 remediation: a review. Journal of Cleaner Production 2014; 77: 10-21.
503 Vidmar J, Oprčkal P, Milačič R, Mladenovič A, Ščančar J. Investigation of the behaviour of
504 zero-valent iron nanoparticles and their interactions with Cd2+ in wastewater by single
505 particle ICP-MS. Science of The Total Environment 2018; 634: 1259-1268.
506 Wan H, Briot NJ, Saad A, Ormsbee L, Bhattacharyya D. Pore functionalized PVDF membranes
507 with in-situ synthesized metal nanoparticles: Material characterization, and toxic
508 organic degradation. Journal of membrane science 2017; 530: 147-157.
509 Wang C, Luo H, Zhang Z, Wu Y, Zhang J, Chen S. Removal of As (III) and As (V) from
510 aqueous solutions using nanoscale zero valent iron-reduced graphite oxide modified
511 composites. Journal of Hazardous materials 2014a; 268: 124-131.
512 Wang X, Chen C, Liu H, Ma J. Preparation and characterization of PAA/PVDF membrane-
513 immobilized Pd/Fe nanoparticles for dechlorination of trichloroacetic acid. Water
514 research 2008; 42: 4656-4664.
515 Wang Z, Cui Y, Wang J, Yang X, Wu Y, Wang K, et al. The effect of thick fibers and large
516 pores of electrospun poly (ε-caprolactone) vascular grafts on macrophage polarization
517 and arterial regeneration. Biomaterials 2014b; 35: 5700-5710.

518 Woo YC, Kim Y, Shim W-G, Tijing LD, Yao M, Nghiem LD, et al. Graphene/PVDF flat-sheet
519 membrane for the treatment of RO brine from coal seam gas produced water by air gap
520 membrane distillation. Journal of Membrane Science 2016; 513: 74-84.
521 Woo YC, Tijing LD, Park MJ, Yao M, Choi J-S, Lee S, et al. Electrospun dual-layer nonwoven
522 membrane for desalination by air gap membrane distillation. Desalination 2017; 403:
523 187-198.
524 Yao M, Ren J, Akther N, Woo YC, Tijing LD, Kim S-H, et al. Improving membrane distillation
525 performance: morphology optimization of hollow fiber membranes with selected non-
526 solvent in dope solution Revised manuscript for Chemosphere. Chemosphere 2019.
527 Zeng Z, Yu D, He Z, Liu J, Xiao F-X, Zhang Y, et al. Graphene oxide quantum dots covalently
528 functionalized PVDF membrane with significantly-enhanced bactericidal and
529 antibiofouling performances. Scientific reports 2016; 6: 20142.